# SPECTRAL ANALYSIS IN THE UV-VISIBLE RANGE FOR REVEALING THE MOLECULAR FORM OF COMBUSTION-GENERATED CARBONACEOUS SPECIES

**C. Russo*, F. Stanzione**, M. Alfè**, A. Ciajolo** and A.Tregrossi****
lina.russo@virgilio.it
*Dipartimento Ingegneria Chimica, Università di Napoli "Federico II"
**Istituto di Ricerche sulla Combustione, CNR, Piazzale Tecchio, 80, 80125 Napoli, Italy

## Abstract
The optical properties of carbonaceous species are object of research across different scientific fields as astrophysics, solid-state physics, atmospheric chemistry and physics, materials, petrology and combustion. Indeed, they are important to the aim of: identifying the composition of interstellar matter, evaluating the air quality and the relative impact on human health and climate change, determining properties of petroleum macromolecules, controlling the production of amorphous carbon-based materials, measuring soot loading and heat transfer in combustion aerosols.
In this work a method of analysis of UV-Visible spectra of combustion-generated carbonaceous species was developed for investigating the relationship between the spectral features and the complex composition of carbonaceous species.
The UV-Visible spectra of carbonaceous species, caught on quartz plates inserted along the axis of ethylene fuel-rich premixed flame, were measured. The contribution of the main components (dry soot and condensed organic species adsorbed on it) was firstly evaluated by measuring the UV-Visible spectra of the deposited particulate matter before and after treatment with dichloromethane (DCM).
A deeper investigation of the contribution of components having different molecular weight (MW) was performed by Size Exclusion Chromatography (SEC) of the dry soot and DCM-soluble fractions and on-line measurements of UV-Visible spectra of MW-segregated fractions. These spectra were used for evaluating: i) the optical band gap of each MW-segregated fractions and ii) the UV peak position of the components of particulate matter by means of a deconvolution procedure of the dry soot and DCM-soluble species spectra.
Structural information on the absorbers were obtained associating each band gap value with the relative UV peak position, very sensitive to the $sp^2$ and $sp^3$ sites and to the size and stacking of the aromatic units of the carbon network. Overall, this procedure has shown to be able to discriminate the contribution of the different components of particulate matter giving information on their molecular form.

## Introduction
The internal structure of carbonaceous species strictly relates to their optical properties, particularly to the UV-Visible absorption that is an useful diagnostic tool for identifying the composition of interstellar matter, for evaluating the impact on human health and climate change of particulate, determining properties of petroleum macromolecules, controlling the production of amorphous carbon-based materials, measuring soot loading and heat transfer in combustion aerosols.
The UV-Visible spectra of carbon particles usually exhibit a broad ($\pi$-$\pi^*$) peak, due to $sp^2$ hybridization and located in the UV between 200 and 250nm, merging with the long

wavelength tail of the (σ-σ*) band, located in the far UV toward 100nm and typical of $sp^3$ carbon sites [1].

In principle, the (π-π*) band position of carbon-based material should be merely related to the $sp^2/sp^3$ character, in particular it has been assessed that the (π-π*) band position shifts toward the visible as the $sp^2$ character increases and the growth of the graphene $sp^2$ layers occurs [2,3,1] allowing to follow the graphitization process occurring in pyrolysis and combustion systems. However, it has to be underlined that other structural parameters as the number of stacked graphitic layers [4] and the curvature of aromatic layers [5] affect the (π-π*) band position. The increase of these structural parameters, also occurring during the graphitization process, causes the shift toward the UV region of the band position in opposition to the shift toward the visible caused by the graphene size growth.

In regard to the graphene $sp^2$ size, the energy band gap measured on the UV-Visible spectra of amorphous carbons following the Tauc optical band gap model [6] has been used by to provide information on the molecular weight (MW) and size (La) of the aromatic islands [7, 8]. The UV absorption model used by Robertson, however, considers only the largest graphene layers to be responsible for the (π-π*) electronic transition feature. Therefore, it fails to describe the internal structure of carbon materials containing graphene layers with a variety of sizes and shapes and does not account for the broadening of the band due to the contributions of the electronic transitions between the small $sp^2$ clusters [1]. Indeed, the carbonaceous species formed in fuel-rich combustion conditions and emitted in the atmosphere have shown a very complex morphology from the macrostructure to micro- and nano-structure. Even in the length scale of nanometers, the aromatic units of different size (>2 rings) can be arranged in non-stacked and stacked units from 2 to 5 stacks giving rise to a different degree of crystalline order [9]. This structural complexity affects the electronic interactions and has to be taken into account for the interpretation of UV-Visible spectral features as the band position and the optical band gap.

The contribution of absorbers having different molecular weight to the UV-Visible spectra of combustion-generated carbonaceous species has been confirmed in early work by evaluating optical band gaps in different wavelength regions of the UV-Visible extinction spectra measured in fuel-rich premixed flames of benzene [10]. In recent work the different optical band gaps of the particulate caught on a quartz plate inserted in flames have been assigned to absorbers having specific molecular weight on the basis of Size Exclusion Chromatography (SEC) of carbonaceous species coupled with on-line UV-Visible spectroscopy [11]. This approach was applied just to the solid carbon particulate devoid of the condensed organic species soluble in dichloromethane (DCM). However the latter ones can represent a significant fraction of the total particulate matter particularly in the early phases of particulate matter formation and in the atmospheric conditions where carbon particles act as condensation nuclei for volatile organic compounds.

In this work, UV-Visible spectral features of combustion-formed carbonaceous species caught on quartz plates inserted along the axis of an ethylene fuel-rich premixed flame have been analyzed taking into account for the contribution of the main components (dry soot and condensed organic species adsorbed on it). Moreover, UV-Visible spectra of MW-segregated fractions of the dry soot and DCM-soluble fractions, as separated by SEC, have been measured and used for evaluating the optical band gap of each MW-segregated fraction and to get the UV band position of the particulate components by means of a purposely-developed deconvolution procedure.

## Experimental techniques

*Sample Preparation*

Combustion-generated carbonaceous species were sampled in an atmospheric-pressure fuel-rich premixed $C_2H_4/O_2$ flame (C/O ratio=0.8, cold gas velocity $v_o$=4cm/s, Tmax=1690K) produced on a commercial McKenna burner (Holthuis & Associates, Sebastopol, CA). The carbonaceous species have been caught on quartz plates inserted into the flame at different heights above the burner (HAB) for the minimum time (400ms) required to collect the amount of material sufficient for the characterization and to reduce the thermal degradation due to the exposition of the deposited sample to the flame [11].

The organic compounds condensed on the deposited carbonaceous species were separated from the solid carbonaceous species (dry soot) by solubilization in dichloromethane (DCM).

Dry soot was removed from the quartz plates by means of N-methyl-pyrrolidinone (NMP) treatment in ultrasonic bath.

Both the organic compounds dissolved in DCM (DCM-soluble fraction) and dry soot suspended in NMP were recovered for the following characterization.

*Characterization techniques*

Ultraviolet-Visible spectra were measured on a HP8453A spectrophotometer. The UV-Visible spectrum of the carbonaceous species deposited on the quartz plate was measured in the 190-1100nm wavelength range before and after dichloromethane (DCM) treatment in order to obtain respectively the spectrum of total carbon particulate and dry soot devoid of the DCM-soluble fraction.

UV-Visible spectra of the DCM-soluble fraction have been measured in standard 1-cm path-length quartz cells. The UV absorption of DCM limited the wavelength detection range for the spectra acquisition of the DCM-soluble fraction to the 250-1100nm.

Size Exclusion Chromatography (SEC) was carried out for the evaluation of the Molecular Weight (MW) distribution of the DCM-soluble fraction and of dry soot.

A HP1050 High Pressure Liquid Chromatograph (HPLC) using NMP as eluent was used for the SEC analysis. The HPLC was equipped with a Diode Array Detector able to measure on-line UV-visible spectra of the MW-segregated fractions from 250nm up to 600nm. SEC calibration curve for MW evaluation has been based on polystyrene standards (PS) and on carbonaceous samples whose MW has been evaluated from the measured Dynamic Light Scattering particle diameter considering a density of 1.8 g/cm3 and spherical shape [12].

The MW distribution of dry soot and DCM-soluble fraction was measured in a wide MW range (1E5-1E10u) by using a 30cm*7.5mm o.d. Jordi Gel divinylbenzene Solid Bead “non-porous” column (injection volume of 10µl, flow rate 1ml/min, room temperature). However, the lighter components of the DCM–soluble fraction eluted as a single peak below the permeation limit of this column (1E5u) of the “non-porous” column. Thus, a highly cross-linked “individual-pore” (30cm*7.5mm o.d.) PL-gel polystyrene/divinyl benzene column (injection volume of 250µl, flow rate 0.5 mL/min, temperature of 80°C) was used to get the MW distribution of the DCM-soluble fraction in the 100-1E5u range.

## Results and Discussion

The UV-Visible spectral analysis has been carried out on the carbonaceous species produced in a fuel-rich sooting ethylene flame (C/O=0.8) whose structure is reported in previous work [13]. Briefly, in this flame the formation of carbonaceous species starts at 4mm height above the burner (HAB) and increases along the flame attaining to a constant value after 10mm HAB. Consistently with the increasing trend concentration of carbon species and their mass absorption coefficient [14], the UV-Visible spectra showed a general rise of the absorbance signal in the soot formation region up to 10mm HAB.

The UV-Visible spectra of the carbonaceous species deposited on quartz plates inserted at selected heights of the soot formation region of the flame are reported in Fig. 1 (left part). The treatment of the deposited particulate with DCM allows to getting the spectra of dry soot, devoid of the DCM-soluble fraction, also reported in Fig.1. For representation clarity the spectra reported in Fig.1 were shifted on the vertical axis of arbitrary values. Overall, the spectra measured on the particulate before and after DCM treatment exhibit a broad peak in the UV moving toward the visible as the flame height increases. This can be generally attributed to the growth of graphene size and to the increase of $sp^2/sp^3$ character occurring during the particle growth. It is noteworthy that the UV maximum position of the dry soot remaining on the quartz plate after DCM treatment is more shifted toward the UV in respect to the total particulate.

*Optical Band Gap Analysis*

Differences in the shape of the spectra can be evidenced in the Tauc representation by using the energy dependence of the absorption coefficient at the absorption edge with the Tauc relation [6]:

$$\sqrt{AE} = B(E - E_g)$$

(A is the absorbance, E is the energy of the incident photon, B is a constant and $E_g$ is the Tauc optical band gap). Moreover, the Tauc representation of UV-Visible absorption furnishes the optical band gap by extrapolating the linear slope to zero absorption.

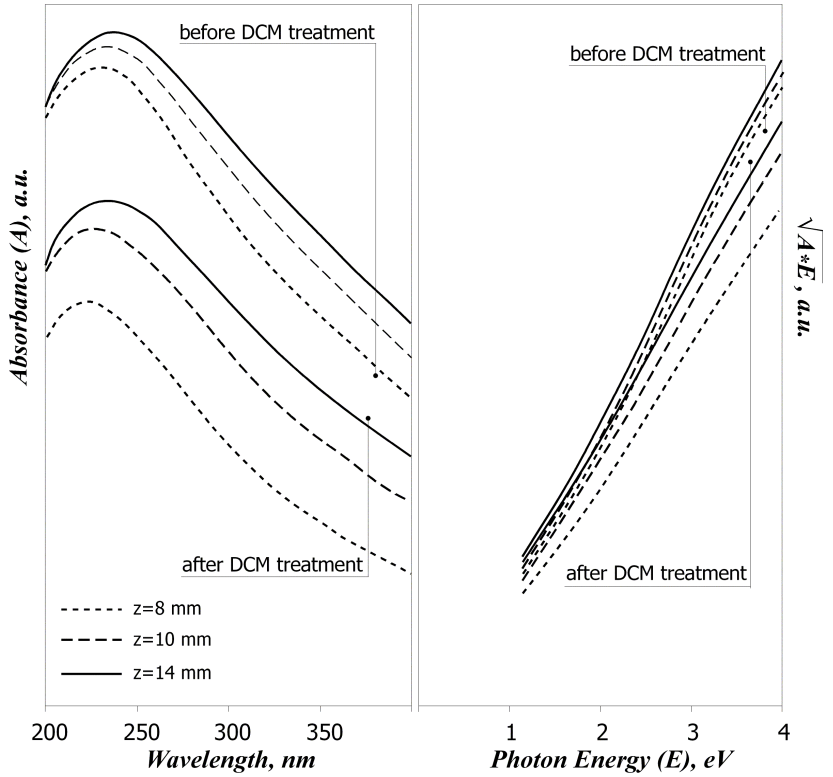


**Figure 1.** The UV-Visible spectra (left part) and Tauc representation (right part) of the carbonaceous species deposited at different HAB before and after DCM treatment.

The absorbance spectra, reported in left part of Fig.1, are represented in the Tauc domain in the right part of Fig. 1, where the square root of A*E is reported as a function of E. In the

Tauc representation it can be noted different spectral features at different flame heights and for effect of the DCM treatment.
It can be also noted that the slope of each absorption curve significantly changes in the visible range and hence, different energy band gaps can be evaluated in dependence on the wavelength region.
This trend is in agreement with previous work [11, 15] where different classes of absorbers having $E_g$ values (0.1-1) typical of large aromatic structures and $E_g$ values (about 2) typical of polycyclic aromatic hydrocarbons with >10 aromatic rings have been detected by optical band gap analysis of benzene and methane soot [11, 15]. A minor contribution of a third class of absorbers having high $E_g$ values (about 4), corresponding to 2- to 7-ring aromatic species, has been also found mainly at the inception of soot and in particular in methane flames [11].
SEC analysis of the DCM-soluble fraction and of dry soot, recovered from the quartz plate, respectively, by DCM treatment followed by NMP treatment, has been performed obtaining the MW distribution and separation in MW-segregated fractions. The SEC system is equipped with a diode array UV-Visible spectrometer able to detect the absorbance signal at fixed wavelengths as well in the UV-Visible range from 250nm up to 600nm..

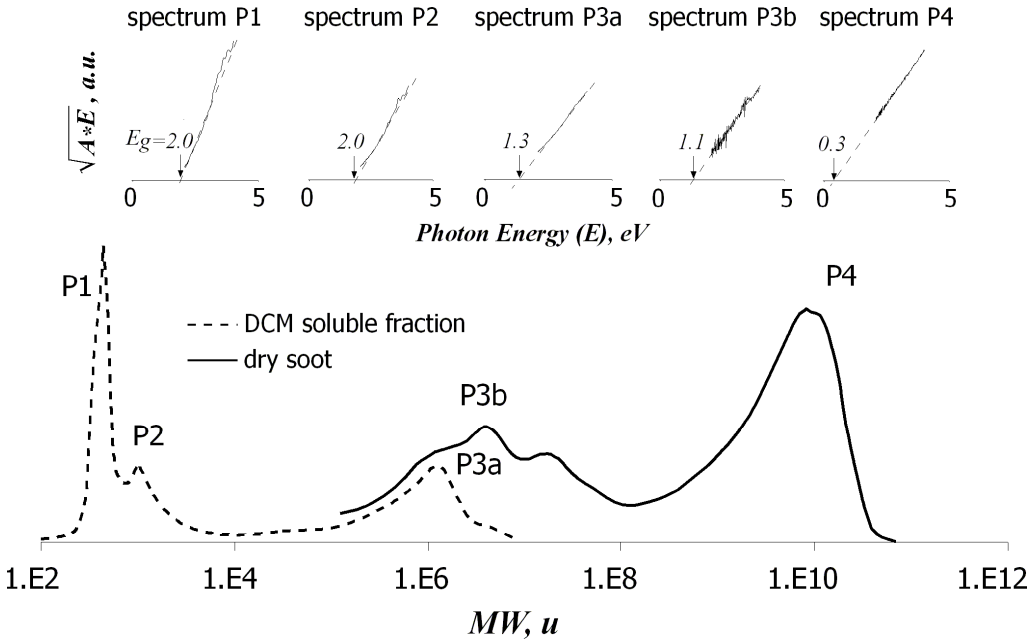


**Figure 2**. MW distribution, obtained by SEC, of the DCM-soluble fraction (dashed line) and dry soot (solid line) sampled at 8mm HAB (lower part) and the band gap evaluated on the spectra of each peak (upper part).

Fig. 2 reports the SEC profile of the DCM-soluble fraction, (measured on the "individual pore" column), joined with the profile of dry soot, (measured on the "non-porous" SEC column), with a detection at fixed 350nm absorption wavelength. The SEC profiles are relative to the sample deposited at 8mm HAB, normalized on their maximum peaks.
The MW distribution of the DCM-soluble fraction covers the low-MW range (200-1E6u) with the predominance of a sharp peak (peak P1) corresponding to a 200-500u MW-segregated fraction and an adjacent smaller peak (peak P2) corresponding to the 500 to 2000u MW-segregated fraction.
The dry soot exhibits a MW distribution of species located in the high-MW range (1E5-1E11u) with a predominant broad peak (Peak P4) from 1E9 to 1E11u.

The MW distributions of the DCM-soluble fraction and dry soot are overlapped in the borderline between the highest MW species of the DCM-soluble fraction (peak P3a) and the lowest MW species of dry soot (peak P3b). It is also noteworthy that the SEC peaks exhibit a broader shape going toward higher MW (from 1E5 to 1E10u). However, the on-line spectra measured in different points of each peak (P3a, P3b and P4), in spite of their broad and structured shape, did not show significant differences both in terms of spectral features and optical band gap.
The Tauc representation of on-line UV-Visible spectra measured of each peak, representing a specific MW-segregated fraction reported in the upper part of Fig. 2, shows that the optical band gap decreases at increasing MW. In particular, the P1 and P2 peaks exhibit the same value ($E_g$=2) typical of large PAH molecules (up to 10-ring pericondensed PAH). The peaks P3a and P3b also exhibit similar values of $E_g$ (about 1) typical of large PAH (tens of condensed aromatic rings) whereas a value of $E_g$=0.3, typical of largely condensed aromatic systems (hundreds of condensed rings), and next to that of graphite (Eg=0) is evaluated for the peak P4.
The similarity of P1 and P2 optical band gaps and of P3a and P3b optical band gaps, in spite of their different MW, indicates that the same aromatic moieties in these species are connected together for giving species with different MW. In other words, P2 peak appears to be composed of clusters of P1 aromatic molecules and P3b is composed of clusters of P3a aromatic species [16].

**Table 1.** Optical band gaps evaluated on the UV-Visible spectra of MW-segregated fractions of DCM-soluble fraction and dry soot at 8, 10 and 14mm HAB. The MW are measured on the maximum of the peaks.

| *Height Above the Burner, mm* | *DCM Soluble Fraction* | | | *Dry Soot* | |
|---|---|---|---|---|---|
| | *spectrum P1 MW ~ 400 u* | *spectrum P2 MW ~ 1000 u* | *spectrum P3a MW ~ 1E6 u* | *spectrum P3b MW ~ 1E7 u* | *spectrum P4 MW ~ 1E10 u* |
| *8* | *2.0* | *2.0* | *1.3* | *1.1* | *0.31* |
| *10* | *2.0* | *2.0* | *1.3* | *1.1* | *0.29* |
| *14* | *2.0* | *2.0* | *1.3* | *1.0* | *0.25* |

It is worth to underline that the SEC profiles of the DCM-soluble fraction and of dry soot did not change at the different flame heights and only the relative increase of the higher MW peaks, and particularly of the P4 peak, was noticed from 8 to 14mm HAB. However the information on structural variations can be obtained from the analysis of the optical band gaps at different flame heights, namely 8, 10 and 14mm HAB, reported in Table 1. It can be observed that the optical band gap values of species belonging to the DCM-soluble fraction (peaks P1, P2 and P3a), as well as the optical band gap value of peak P3b, belonging to dry soot, are quite constant along the flame. On the other hand, the optical band gap of the highest MW species (1E10u), belonging to the dry soot (peak P4), clearly decreases at higher flame heights. Hence, it can be concluded that the species up to a 1E8u do not undergo structural variations, but participate to the growth of particulate concentration by aggregation/coagulation to form large particles from 1E8 to 1E11, instead, undergo dehydrogenation/condensation reactions modifying their internal structure during the particle formation process.

*UV-visible maximum position*

As mentioned before, the position of the UV maximum is another spectral parameter important for defining the internal structure of particulate components. The UV maximum

position can be determined on the spectrum of the dry soot remaining after DCM treatment of the total carbonaceous species deposited on the quartz plate (Fig.1). The UV maximum position of the DCM-soluble fraction can be also determined by considering that the spectrum obtained by difference between the spectra measured on the quartz plate before and after DCM treatment is representative of the DCM-soluble fraction spectrum.
On the other hand, the UV maximum position of each MW-segregated fraction can not be directly determined due to the UV interference of the NMP, used as solvent and eluent for the SEC analysis, that limits the measure of the spectra down to the 290nm wavelength limit. Thus, on the basis of the DCM-soluble fraction and dry soot spectra, measured in the whole 190-600nm range, a deconvolution procedure has been developed for evaluating the contribution of each peak, i.e. each MW-segregated fraction, and their UV maximum position. For the computing procedure the spectra of the MW-segregated fractions, corresponding to the P1, P2, P3a, P3b and P4 peaks, have been considered in the 290-600nm range where the interference of NMP absorption is avoided. In this range the contribution of each MW-segregated fraction was evaluated, minimizing the root-mean-square deviation between the UV-Visible spectra of DCM-soluble fraction and dry soot and the linear combination of the UV-Visible spectra of the relative MW-segregated fractions.
The spectra of the DCM-soluble fraction and of dry soot have been reconstructed in the 190-290nm range using Gaussian functions to be joined with the measured spectra of the MW-segregated fractions in the 290-600nm range. The Gaussian functions have been chosen since they take into account for statistical phenomena such as the electronic properties of carbon materials [1].

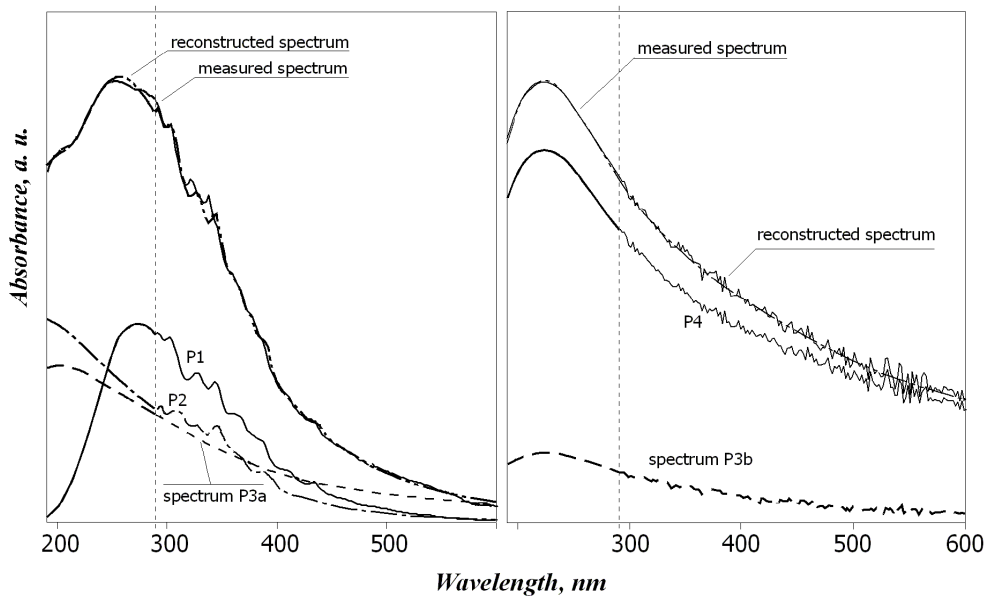


**Figure 3**. The UV-Visible spectra of the DCM-soluble fraction (left part) and dry soot (right part) measured for the 8mm HAB sample, in comparison with the typical output of the reconstruction procedure. Vertical dashed line represents the wavelength (290nm) where the reconstructed spectra and the measured spectra of the MW-segregated fractions are joined.

On this basis the reconstructed spectra have been obtained by minimizing the root-mean-square deviation between the measured spectra and the sum of Gaussian functions for each MW-segregated fraction imposing at 290nm as junction conditions the equality of the

absorbance values and of the first derivatives of the Gaussian functions and of the corresponding MW-segregated fraction measured spectra.
Fig. 3 reports the UV-Visible spectra of the DCM-soluble fraction (left part) and dry soot (right part) measured for the 8mm HAB sample in comparison with the typical output of this reconstruction procedure, i.e. the reconstructed spectrum and the spectra of the MW-segregated fractions in the whole UV-visible range. Table 2 reports the main parameters, as the maximum position and the percentage of absorbance at 350nm for each MW-segregated fraction, evaluated by applying this procedure to all analyzed samples (8, 10 and 14 mm HAB). The UV maximum position calculated for the peak P1 appears to be located at 270nm typical of PAH with more than four rings [17, 18] consistently with the band gap of about 2 (Table 1) that is typical of large PAH. This is in agreement also with the GC-MS analysis of the DCM-soluble fraction that has shown the very low abundance of two-, three-ring PAH and the richness in PAH from four- to seven-ring PAH. Interestingly enough, the flame-formed PAH, as measured by batch-sampling and analysis, have shown to be mainly constituted of light two-three-ring PAH [13], hence it has to be concluded that the light PAH, abundantly formed in flame, escape to the deposition on the quartz plate.
The UV-Visible spectrum of the P2 peak exhibits a broader shape typical of polymeric aromatic materials and the computing procedure did not give out a maximum down to 190 nm, but only an increasing trend of the absorbance profile toward the far UV. As above reported, the MW-segregated fraction, corresponding to the P2 peak, is characterized by the same band gap (Table 1), typical of up to 10-ring aromatic species, and a higher MW (500-2000u) with respect to the P1 peak (200-500u) (Fig.2). Consistently with previous work [19] it can be deduced that the peak P2 includes clusters (dimers or trimers) of P1 aromatics connected by $sp^3$ carbon bonding that, causing the $sp^2/sp^3$ ratio decrease, shifts the maximum absorption position toward the far-UV with respect to P1 peak.

**Table 2.** Maximum absorbance wavelength and absorbance % at 350nm evaluated from the reconstructed UV-Visible spectra of MW-segregated fractions of DCM-soluble fraction and dry soot at 8, 10 and 14mm HAB.

| *Height Above the Burner, mm* | | *DCM Soluble Fraction* | | | *Dry Soot* | |
|---|---|---|---|---|---|---|
| | | *spectrum P1* | *spectrum P2* | *spectrum P3a* | *spectrum P3b* | *spectrum P4* |
| *8* | $\lambda (A_{max})$, *nm* | *273* | *<190* | *200* | *223* | *223* |
| | *Abs%@350nm* | *19.2* | *7.7* | *9.7* | *9.8* | *53.5* |
| *10* | $\lambda (A_{max})$, *nm* | *274* | *<190* | *200* | *223* | *228* |
| | *Abs%@350nm* | *10.0* | *7.1* | *6.1* | *4.7* | *72.1* |
| *14* | $\lambda (A_{max})$, *nm* | *276* | *<190* | *200* | *223* | *235* |
| | *Abs%@350nm* | *4.4* | *2.2* | *5.1* | *3.1* | *85.24* |

The peak P3a, as well as the peak P3b, presents a broad unstructured spectrum and a lower band gap value typical of large (>10 rings) aromatic systems (Table 1). Both the band gap and MW of peak P3a and peak P3b are very similar. The noticeable difference is represented by the computed maximum absorption position of peak P3a spectrum, located at 200nm, that is more shifted toward the UV with respect to peak P3b located at 223nm. This suggests a greater abundance of $sp^3$ carbon in the P3a species that, in turn, can be the reason for the solubilisation in DCM of such higher MW species.
The peak P4 almost completely takes into account for the dry soot absorption spectrum and, as mentioned before, its band gap is very low, typical of large graphitic structures (Table 1).

The UV maximum position of P4 peak clearly moves toward the visible from 220 to 230nm along the flame, confirming the occurrence of graphitization process, suggested by the corresponding band gap decrease from 0.3 to 0.25 (Table 1).
Thus, it can be concluded that the spectral features of carbonaceous species distributed in a wide MW range (from 200 to 1E11u) are mainly affected by the higher MW species/particles included in the 1E8-1E11u MW range. Just these species have shown to undergo graphitization/growth reactions during the soot formation process. The aromatic species of lower MW/size including large PAH and clusters of PAH do not exhibit neither a continuous molecular growth nor an internal structure transformation, but participate to the formation of large particles.

**Conclusions**

The UV-Visible spectra of carbonaceous species, caught on quartz plates inserted along the axis of a premixed sooting ethylene flame were measured. The contribution of the main components (dry soot and condensed organic species adsorbed on it) was evaluated by measuring the UV-Visible spectra of the deposited particulate matter before and after treatment with DCM.
UV-Visible spectra of the dry soot and DCM-soluble fraction and of their MW-segregated fractions, as separated by size exclusion chromatography, were measured for evaluating, for each MW-segregated fraction, the optical band gap that is sensitive to the size of aromatic units. To get the UV maximum position for each MW-segregated fraction a deconvolution procedure was applied to the spectra. Structural information were obtained associating each band gap value to a specific UV maximum position, very sensitive to the $sp^2$ and $sp^3$ sites of the carbon network and to the size and stacking of the aromatic units.
The spectral features of carbonaceous species distributed in a wide range of MW (from 200 to 1E11u) were found to be mainly affected by the higher MW species, included in the 1E8-1E11u range. Just these species showed to undergo graphitization/growth reactions during the formation process of carbonaceous species. The aromatic species of lower MW from large PAH to clusters of PAH included in the 200-1E8u range, did not exhibit neither a continuous molecular growth nor an internal structure transformation, but merely aggregate/coagulate participating to the formation of large carbon particles.
Further work will be focused to systematically apply this approach for studying the effect of fuel identity on the spectral features of carbonaceous species, extending the spectral analysis wavelength range from the vacuum UV to the IR range.

**Acknowledgments**

This work was supported by Ministero dello Sviluppo Economico within the Accordo di Programma MSE-CNR-Gruppo Tematico “Carbone Pulito”, 2010.

**References**

[1] Llamas-Jansa, I, Jäger, C., Mutschke, H, Henning, Th., “Far-ultraviolet to near-infrared optical properties of carbon nanoparticles produced by pulsed-laser pyrolysis of hydrocarbons and their relation with structural variations”, *Carbon* 45: 1542-1557 (2007)

[2] Tomita, S., Fujii, M., Hayashi, S., “Defective carbon onions in interstellar space as the origin of the optical extinction bump at 217.5 nanometers”, *The astrophysical Journal* 609: 220-224 (2004)

[3] Mennella, V., Colangeli, L., Bussoletti, E., Merluzzi, P., Monaco, G., Palumbo, P. Rotundi, A., "Laboratory experiments on cosmic dust analogues: the structure of small carbon grains", *Planet. Space Sci.* 43: 1217-1221 (1995)
[4] Duley, W. W., Seahra, S., "Graphite, polycyclic aromatic hydrocarbons, and the 2175 Å extinction feature", *The Astrophysical Journal* 507: 874-888 (1998)
[5] Henning, Th., Jäger, C., Mutschke, H, "Laboratory Studies of Carbonaceous Dust Analogs", *Astrophysics of Dust* 309: 603-628 (2004)
[6] Tauc, J., Grigorovici, R., Vancj, A., "Optical properties and electronic structure of amorphous germanium", *Phys. Stat. Sol*. 15: 627-637 (1966)
[7] Robertson, J., "Hard amorphous (diamond-like) carbons", *Prog. Solid St. Chem*. 21: 199-333 (1991)
[8] Robertson, J., O'Reilly, E.P., "Electronic and atomic structure of amorphous carbon", *Phys. Rev B* 35: 2946-2957 (1987)
[9] Galvez, A., Herline-Boime, N., Reynaud, C., Clinard, C., Rouzaud, J. N., "Carbon nanoparticles from laser pyrolysis", *Carbon* 40: 2775-2789 (2002)
[10] Minutolo, P., Gambi, G., D'Alessio, A., "The optical band gap model in the interpretation of the uv-visible absorption spectra of rich premixed flames", *Proc. Comb. Inst.* 26: 951-956 (1996)
[11] Tregrossi, A., Ciajolo, A., "Spectral Signatures of carbon particulate evolution in methane flames", *Combust. Sci. and Tech.* 182: 683-691 (2010)
[12] D'Anna, A., Ciajolo, A., Alfè, M., Apicella, B., Tregrossi, A., "Effect of fuel/air ratio and aromaticity on the molecular weight distribution of soot in premixed n-heptane flames", *Proc. Comb. Inst.* 32:803-810 (2009)
[13] Apicella, B., Barbella, R., Ciajolo, A., Tregrossi, A. "Formation of low- and high-molecular-weight hydrocarbon species in sooting ethylene flames" *Combust. Sci. and Tech*. 174: 309-324 (2002)
[14] Alfe, M., Apicella, B., Rouzaud, J. N., Tregrossi A.; Ciajolo A.; "The effect of temperature on soot properties in premixed methane flames" *Combust. Flame* 157: 1959-1965 (2010)
[15] Russo, C., Stanzione, F., Barbella, R., Tregrossi A.; Ciajolo A.; "The Characteristics of soot formed in premixed flames by different fuels" *Chemical Engineering Transactions* 22: 41-46 (2010)
[16] Sirignano, M., Alfè, M., Tregrossi, A., Ciajolo, A., D'Anna, A., "Experimental and modeling study on the molecular weight distribution and properties of carbon particles in premixed sooting flames", *Proc. Comb. Inst.* 33: 633-640 (2011)
[17] Wasserfallen, D., Kastler, M., Pisula, W., Hofer, W. A., Fogel, Y., Wang, Z., Müllen, K., "Suppressing Aggregation in a Large Polycyclic Aromatic Hydrocarbon", *J. Am. Chem. Soc.* 128: 1334-1339 (2006)
[18] Fetzer, J. C., *Large (C>=24) polycyclic aromatic hydrocarbons*, Wiley & Sons, 2000, p. 67
[19] Alfè, M., Apicella, B., Tregrossi, A., Ciajolo, A., "Identification of large polycyclic aromatic hydrocarbons in carbon particulates formed in a fuel-rich premixed ethylene flame", *Carbon* 46: 2059-2066 (2008).